

Articles

Investigations of Neurotrophic Inhibitors of FK506 Binding Protein via Monte Carlo Simulations

Michelle L. Lamb and William L. Jorgensen*

Department of Chemistry, Yale University, New Haven, Connecticut 06520-8107

Received January 27, 1998

The binding and solution-phase properties of six inhibitors of FK506 binding protein (FKBP12) were investigated using free energy perturbation techniques in Monte Carlo statistical mechanics simulations. These nonimmunosuppressive molecules are of current interest for their neurotrophic activity when bound to FKBP12 as well as for their potential as building blocks for chemical inducers of protein dimerization. Relative binding affinities were computed and analyzed for ligands differing by a phenyl ring, an external phenyl or pyridyl substituent, and a pipercolyl or prolyl ring. Such results are, in general, valuable for inhibitor optimization and, in the present case, bring into question some of the previously reported binding data.

Introduction

The α -ketoamide functionality of the immunosuppressant natural product FK506 (Figure 1) is retained in many of the highest affinity ligands that have been developed to inhibit the rotamase (cis–trans peptidyl-prolyl isomerase, or PPIase) activity¹ of the FK506 binding protein (FKBP12, MW = 12 kDa).² Originally, interpretation of the crystal structure of FK506–FKBP12 led to the belief that the α -ketoamide mimics a twisted-amide transition state of peptide bond isomerization, although an endogenous substrate for FKBP12 had not been discovered. It was thought that blockage of the isomerase active site prevented modification of downstream proteins necessary for T-cell activation, and this was the source of the observed immunosuppression. A similar mechanism had been proposed for the activity of the undecapeptide cyclosporin A (CsA), which inhibits the PPIase cyclophilin, although neither the natural products nor the proteins are homologous. However, evidence that rotamase inhibition was not sufficient for immunosuppression soon began to mount.³ Rapamycin (Figure 1), another fungal molecule structurally similar to FK506, inhibited FKBP12 but appeared to influence a later stage of the T-cell cycle. Schreiber and co-workers⁴ made a significant contribution with the synthesis of a molecule which retained the FKBP12 binding domain of FK506 and rapamycin (pyranose ring, α -ketoamide, pipercolate ester, and cyclohexyleth(en)yl groups), but in which the macrocycle was contracted. This molecule was a rotamase inhibitor but did not prevent T-cell proliferation.

It later became clear that the formation of an immunosuppressant–immunophilin complex results in a gain of function for the protein. The CsA–cyclophilin and FK506–FKBP12 pairs each present a recognition surface to the calcium-dependent, serine/threonine phosphatase, calcineurin (CN).⁵ The FK506–FKBP12 complex binds at least 10 Å from the active site of CN and

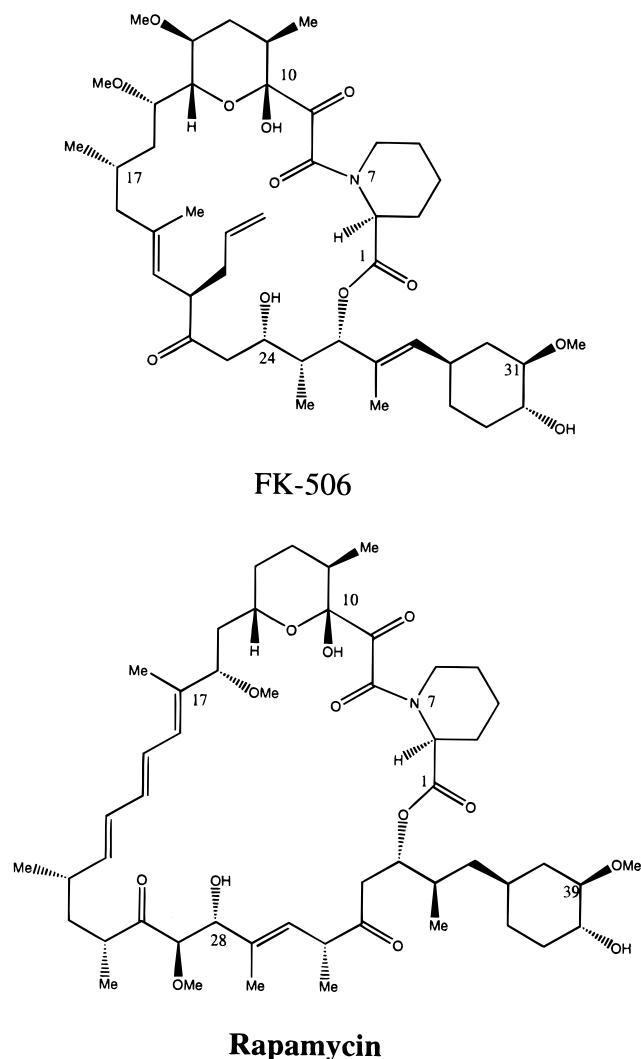
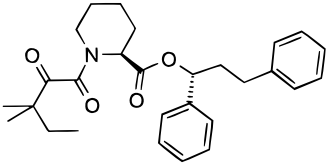
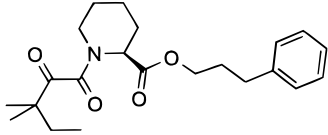
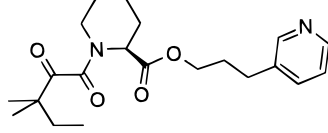
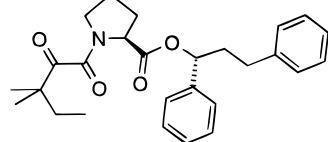
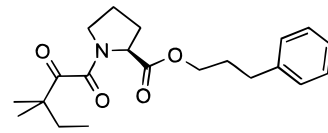
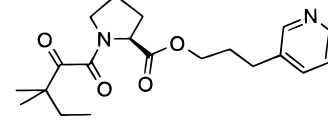


Figure 1. Structures and atom numbering for the immunosuppressants FK506 and rapamycin.

Table 1. Experimental Activities for Selected FKBP12 Ligands

compd	structure	rotamase K_i , nM	neurite outgrowth ED_{50} , nM ^a
1		17 ^b , 10 ^c	0.3
2		250 ^b , 110 ^c	300
3		130 ^b , 165 ^c	8.5
4		52 ^b	—
5		42 ^b	53
6		7.5 ^b	0.05

^a Data on neurite outgrowth from chick dorsal root ganglia reported in ref 2. ^b Data from Guilford Pharmaceuticals, refs 2 and 59. ^c Data from SmithKline Beecham, refs 13 and 16.

must block binding of subsequent phosphorylated proteins and thus the T-cell signaling pathway.^{6,7} Reports of the association of calcium channels containing -Leu-Pro- sequences with both FKBP12 and CN are filling in another long-standing piece of the FKBP12 puzzle, as these may represent endogenous "ligands" for FKBP12 mimicked by FK506.⁸ In contrast, rapamycin-FKBP12 interrupts a distinct signaling cascade through its interaction with another protein, generally termed FRAP (FKBP-rapamycin-associated protein).⁹⁻¹¹ A crystallographic structure of this ternary complex confirms the recognition requirements for rapamycin.¹² In both FKBP12 ligands, it is the portion of the macrocycle opposite the α -ketoamide-pipecolic acid moiety, the "effector" region, which contacts calcineurin.

As part of an effort to design low molecular weight PPIase inhibitors as scaffolds for the immunosuppressive effector components, the crystal structure of **1**-FKBP12 (Table 1) was solved at SmithKline Beecham in 1993.¹³ Figure 2 shows the binding mode revealed for the α -ketoamide and pipercolyl portion of **1**. The keto carbonyl (O4) contacts aromatic hydrogens of Tyr²⁶, Phe³⁶, and Phe⁹⁹, and the pipercoline ring sits over Trp⁵⁹. The 3-phenylpropyl moiety binds in the solvent-exposed FK506-cyclohexyl groove of FKBP12 between Ile⁵⁶ and

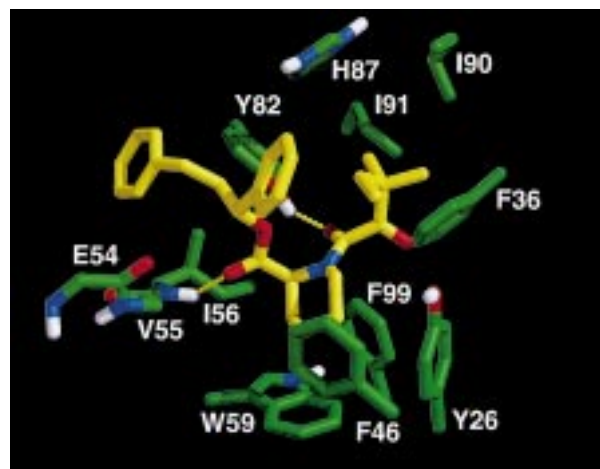


Figure 2. Position of compound **1** (yellow) in the aromatic binding pocket of FKBP12 (green).¹³ Molecular graphics images were produced using the MidasPlus software system from the Computer Graphics Laboratory, University of California, San Francisco.⁶⁰

Tyr⁸², and these residues form hydrogen bonds with the ester (O2) and amide (O3) carbonyl oxygens of the ligand. The 1-phenyl substituent interacts with Phe⁴⁶ and the tertiary pentyl group of the inhibitor. A

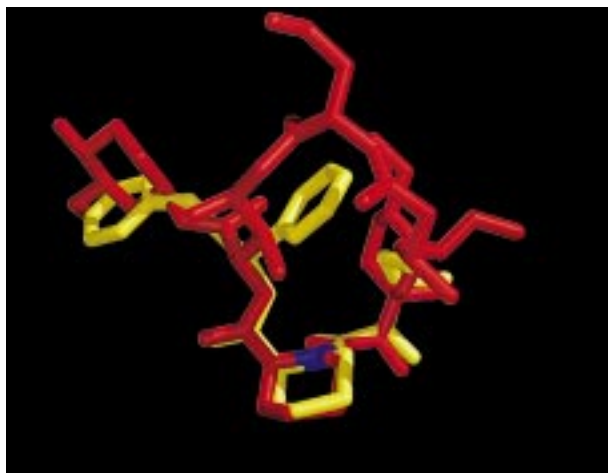
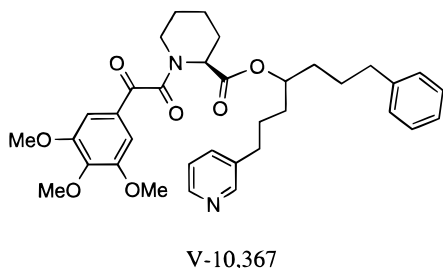


Figure 3. FKBP12-bound conformation of **1** (yellow) overlaid with that of FK506 (red).^{13,15}

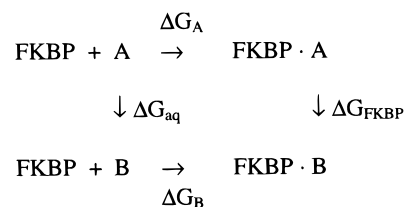
comparison of the bound conformation of **1** and FK506 presented in Figure 3 demonstrates that this mode is consistent with that found in crystallographic structures of FK506–FKBP12 and rapamycin–FKBP12.^{14,15} However, the ability to form hydrogen bonds to the Glu⁵⁴ carbonyl observed in complexes with FK506 (C24–OH) and rapamycin (C28–OH) is not present in this ligand. Binding patterns similar to those for **1** may be expected for compounds **2** and **3** (Table 1) as well.^{13,16} An excellent analysis of FKBP12–ligand interactions, including discussion of previously unpublished atomic structures, is included in a review of protein–ligand recognition motifs by Babine and Bender.¹⁷

An additional activity for rotamase inhibitors of this class has expanded interest in these compounds beyond their potential in immunosuppressant drug design. As reviewed recently by Hamilton and Steiner,² FK506 has been shown to induce the regeneration of damaged nerves in animal models of Parkinson's and Alzheimer's diseases. Furthermore, the enriched concentration of FKBP12 in neurons has been associated with nitric oxide synthesis, neurotransmitter release, and neurite extension. Potent, nonimmunosuppressive FKBP12 ligands, such as V-10,367^{18–20} and GPI-1046 (**6**, Table



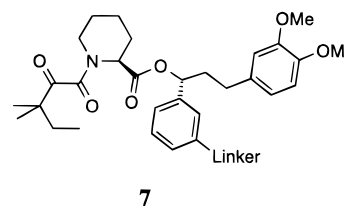
1),^{21–23} are able to promote neuronal growth in vitro and in vivo without the addition of exogenous growth factors. They have a better therapeutic potential than growth factors in that they are orally bioavailable and able to cross the blood–brain barrier. The requirement of binding to FKBP12 for neuronal activity has also been demonstrated, but there is no linear relationship between rotamase inhibition and activity in neuronal cells.² FKBP12 binding is apparently necessary but not sufficient for stimulation of nerve growth, suggesting

Scheme 1



that, as in T-cells, the complex may modify the function of an additional target.

Another use of this class of FKBP12 ligands has also emerged. The ability of the immunosuppressants to induce protein heterodimerization and the knowledge of ligand modifications that prevent this association has been exploited for control of cellular signaling pathways, protein translocation, and gene activation.^{24,25} Target proteins are first artificially attached to the immunophilins (FKBP12 or cyclophilin), CN, or FRAP. The ligands themselves or synthetic homo- or heterodimers of FK506, CsA, or rapamycin then bring their protein partners together, resulting in the proximity of the target proteins and transmission of signal.^{24–30} Recently, dimers of **7** have been used to effect cellular apoptosis and to induce transcription, again without the immunosuppressive effects of further binding to calcineurin.³¹ This technique of “chemically induced dimerization”, used with small, cell-permeable molecules such as **7**, is



designed to have application in cellular gene therapy.

Given the diverse biological applications of these α -ketoamide ligands and that only slight differences in structure can have profound effects on activity, we have used theoretical techniques to probe the binding of compounds **1–6** (Table 1) at the atomic level, in both structural and energetic terms. Previous simulations of FKBP12 have addressed the rotamase mechanism applied to peptide substrates^{32,33} and the importance of Tyr⁸² in binding FK506.³⁴ Our current approach has focused on free energy perturbation (FEP) calculations, using Monte Carlo (MC) methods rather than molecular dynamics (MD) for sampling. Computed relative free energies of binding, which are obtained from simulations of the ligands in solution and bound to the protein, may be compared with those obtained from experimental binding constants (Scheme 1). Averages of the computed structures may then be used to analyze the origin of the differences in binding affinities.

The MC method used here has been validated with a study of benzamidine inhibitors of trypsin³⁵ and was further applied to the analysis of orthogonal CsA–cyclophilin pairs as components of a system for chemically induced dimerization.³⁶ The present study is aimed at understanding factors that influence the binding of **1** and its analogues. In particular, the effects of removal of the 1-phenyl group, conversion of the 3-phenyl to 3-(3-pyridyl), and ring contraction of the

pipecolyl ring to prolyl are examined. There are discrepancies in the binding data from the two experimental sources, as indicated by the results for **2** and **3** in Table 1. From the crystal structure for **1** bound (Figure 2), the pyridine nitrogen of **3** is anticipated to be solvent exposed. Thus, it would normally not be expected to favor the lower dielectric environment of a protein ($\epsilon \approx 4$) over that of bulk water ($\epsilon \approx 80$),³⁷ in contrast to the binding results from Guilford Pharmaceuticals. This was pursued through computations for the **2**, **3** and **5**, **6** pairs. Hamilton and Steiner have also pointed out that **5** and **6** are the first examples of prolyl compounds that bind better than their pipecolyl analogues, but the high affinity is attributed only to "improved design".² To investigate further, differences in free energies of binding were computed for two pairs of pipecolyl and prolyl ligands. Compounds **2** and **5** represent the unusual case with the prolyl ligand (**5**) as the better inhibitor. Compounds **1** and **4** represent the more common situation in which the presumably more hydrophobic pipecolyl ligand (**1**) has higher affinity for FKBP12.

Computational Details

Parametrization and Initial MC Simulations.

The crystal structure of **1**-FKBP12 at 2.0 Å resolution¹³ from the Brookhaven Protein Data Bank³⁸ (entry 1fkg) was used as the starting point for the simulations. The computational protocol for the MC simulations was the same as in previous applications.^{35,36} The good precision that is obtainable for free energy changes with this methodology was addressed extensively in ref 35. The MC sampling included variation of all bond angles and dihedrals of the ligand and protein side chains as well as overall rotation and translation of the ligand and water molecules. The protein backbone atoms were held fixed in their crystallographic positions. This makes the MC simulations more rapid, and the approximation is justified for FKBP12. Restricted backbone motion on the picosecond time scale has been noted for native FKBP12,³⁹ and ligand binding further rigidifies the protein structure, as demonstrated by the close resemblance among atomic structures of FKBP12 in numerous FKBP12-ligand complexes.¹⁷ To be consistent with prior MD calculations on the FK506-FKBP12 system,⁴⁰ all 79 residues within 12 Å of FK506 in its cocrystal structure with FKBP12¹⁴ were sampled. This provided a greater number of moving side chains than would be found in a 12 Å region around **1**.

The OPLS united-atom force field⁴¹ with all-atom aromatic groups⁴² provided most parameters for the protein; parameters for the inhibitors also came from this source and from a previous MD study of FK506.⁴³ A listing of parameters for the inhibitors is provided in the Supporting Information. The torsional parameters for the amino acid residues were derived from fitting to torsional energy profiles obtained from ab initio calculations with the 6-31G* basis set.⁴⁴ Any missing parameters were derived by fitting to MM2⁴⁵ energy profiles, which were generated using MacroModel.⁴⁶ A scale factor of 1/2 was applied to all 1-4 nonbonded interactions. Histidines 25, 87, and 94 are known to be unprotonated,⁴⁷ and they were designated as δ -tautomers based on visual inspection. This tautomeric state has

also been chosen in MD simulations of FKBP12-ligand complexes in solution.^{32,34}

The unbound ligands and protein-ligand complexes were solvated with 22 Å spheres containing 1477 and 939 TIP4P water molecules, respectively. A half-harmonic potential with a 1.5 kcal/mol Å² force constant was employed to prevent waters from migrating away from the cluster. A 9 Å residue-based cutoff was used for all nonbonded interactions; if any pair of atoms from two residues was within this distance, all nonbonded interactions between the residues were included in the energy evaluation. The list of nonbonded interactions was updated every 2×10^5 configurations during the simulations.

All Monte Carlo simulations were performed with the MCPRO program.⁴⁸ An advantage of using internal coordinate MC methods is the ability to focus sampling on specific regions and degrees of freedom of interest. Consequently, bond lengths were fixed to their crystal structure values, and aromatic rings were treated as rigid units. To prevent inversion at sp³ centers such as α -carbons and to enforce planarity of sp² centers for more efficient sampling, improper dihedral angles were not varied except as noted below. Otherwise, all bond angles and dihedrals in the moving portion of the system were sampled.

The MC simulations were carried out for 25 °C on Silicon Graphics workstations and on a cluster of personal computers using Pentium processors. It may be noted that the experimental results come from an assay for rotamase inhibition.⁴⁹ This widely used procedure for measuring FKBP12 binding affinities is usually performed somewhat below room temperature, e.g., near 10 °C.¹³ The solvent was first sampled for 1 million (*M*) configurations to remove any highly repulsive initial contacts with the solutes. Then, 8*M* configurations were performed to equilibrate the **1**-FKBP12 complex. The same protocol was followed for **1** in solution, beginning with the bound conformation taken from the **1**-FKBP12 structure. During equilibration, the conformation of the bound ligand remained similar to the crystal conformation; however, partial inversion of the pipecolyl ring occurred in solution to switch it from a chair to a half-chair conformation (Figure 4). In gas-phase optimizations of ligand **1** with the present force field, the adopted ring conformation is favored by 1.3 kcal/mol. This is likely an artifact of using the AMBER C2-N-CH bending parameters with $\theta_0 = 118^\circ$, which was not designed for a piperidine ring.⁵⁰ The difference is expected to have little effect on the computed free energy changes since the mutated phenyl rings are not in contact with the pipecolyl ring or, in the case of the ring contraction, the chair conformation was enforced (vide infra).

Free energy changes were calculated during the MC simulations according to standard procedures of statistical perturbation theory.⁵¹⁻⁵³ The difference in free energy of binding ($\Delta\Delta G_b$) for molecule B relative to molecule A (Scheme 1) may be obtained from transformations of the ligands in solution and bound to the protein according to eq 1:

$$\Delta\Delta G_b(A \rightarrow B) = \Delta G_B - \Delta G_A = \Delta G_{\text{FKBP}} - \Delta G_{\text{aq}} \quad (1)$$

FEP Simulation Protocol for 1→2. This perturba-

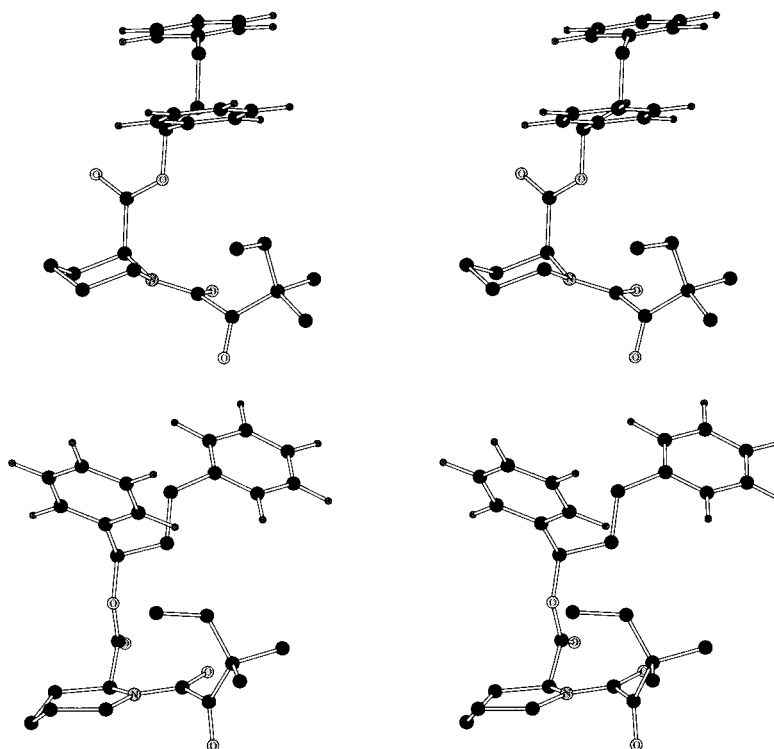


Figure 4. Stereoviews of unbound ligand **1**. The initial geometry from the **1**-FKBP12 crystal structure has the pipecolic ester substituent in an axial conformation (top). Subsequent equilibration resulted in partial inversion of the ring (bottom).

tion involved the removal of the 1-phenyl ring of **1** to obtain **2**. The atoms of the phenyl group were converted to "dummy" atoms without charge or Lennard-Jones parameters, and the length of the bond connecting the substituent to the remainder of the ligand was reduced to 0.65 Å with all other phenyl ring bonds reduced to 0.35 Å. The transformation of **1**→**2** was carried out in 13 windows with double-wide sampling, which yield 26 free energy increments.⁵¹ A coupling parameter, λ , was employed such that $\lambda = 0$ corresponds to the initial state, **1**, and $\lambda = 1$ corresponds to the final state, **2**. The first six windows used $\Delta\lambda = \pm 0.025$, while the remaining windows used $\Delta\lambda = \pm 0.050$. All were equilibrated with 2–4M configurations of sampling; the last configuration of the previous window was used to start the next one. Averaging was done in batches of 2×10^5 configurations, with data collected over a total of 4–7M configurations in each window. For subsequent analyses of hydrogen bonding, an additional 1M configurations were generated at the endpoints of the simulations.

FEP Simulation Protocol for 2→3, 5→6. The next transformation addressed was the conversion of a phenyl moiety to a 3-pyridyl ring. This perturbation is straightforward; the analogous perturbation of benzene to pyridine had been performed in the development of OPLS all-atom (OPLS-AA) parameters for pyridine.⁵⁴ As before, the standard phenyl ring structure was transformed to a pyridine geometry determined from microwave experiments.⁵⁴ A model of **5** was required prior to the conversion of **5**→**6** and was obtained by mapping a prolyl ring onto the final structure of **2** from the **1**→**2** FEP calculation. In each simulation, the prolyl or pipecolyl ring was flexible. The perturbation protocol for these calculations was slightly modified from that

used for **1**→**2** to take advantage of the acquisition of a new parallel computing system within our laboratory. Seven double-wide windows were run in parallel, with 4–8M configurations sampled during the equilibration phase and with data collected over 4–12M configurations. A gas-phase FEP calculation was also performed for **5**→**6** to allow estimation of the relative free energies of hydration of the two ligands.

FEP Simulation Protocol for 2→5, 1→4. In our experience, perturbations between different cyclic systems require much care to implement and can be particularly slow to converge. The necessity of accounting for both changes in bonded and nonbonded interactions within the ring as one atom disappears makes this a technically difficult perturbation. One way to simplify the present calculations is to drive the ring from one fixed six-membered ring conformation to a fixed five-membered ring conformation, "disappearing" the remaining atom and simultaneously reeling it in toward the others. For this rigid perturbation, changes in energy within the ring need not be monitored, as these intraligand differences should be very similar in each environment (bound and unbound). However, other possible conformations for the rings would not be taken into account, and the results could be sensitive to the path chosen.

The simulations for the unbound and bound transformations were started from the final *bound* conformations of **2**-FKBP12 or **1**-FKBP12 above with the chair conformation for the pipecolyl ring. The final prolyl ring geometry was obtained from a gas-phase optimization of the bound conformation of **2** with one ring atom converted to a dummy atom, as illustrated in Figure 5. Other than for the internal structures of the pipecolyl and prolyl rings, the sampling for the ligands included

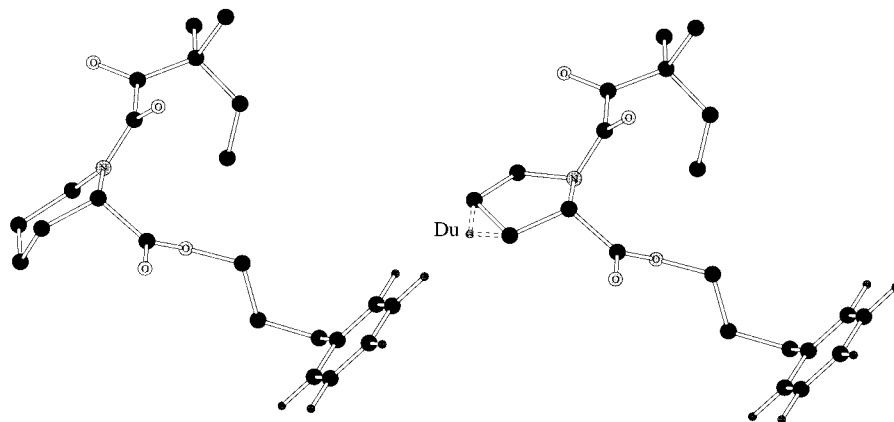


Figure 5. The initial and final ring conformations of the 2→5 perturbation. The dummy atom in 5 is noted Du.

all bond angles and dihedral angles, as before. Prior to the FEP calculation, the unbound ligands, **2** and **1**, were each resolvated and relaxed with 4.4M configurations of solvent-only sampling, followed by 8M configurations of full equilibration. Twenty-one windows were used to perform the ring contraction in small steps. Fortunately, convergence was rapidly achieved within the 4M configurations performed for both equilibration and averaging.

Results and Discussion

Effect of the 1-Phenyl Group, 1→2. Removal of the 1-phenyl moiety from **1** is a large perturbation but a computationally attractive choice given the available structural information and the sizable difference in binding affinity (Table 1). The free energy change as a function of λ from the FEP calculations for the unbound and bound ligands proceeded smoothly (Figure 6a), with $\Delta G_{\text{aq}} = 10.25 \pm 0.31$ kcal/mol and $\Delta G_{\text{FKBP}} = 11.69 \pm 0.31$ kcal/mol (Table 2). The resultant relative free energy of binding ($\Delta\Delta G_b$) of 1.4 kcal/mol obtained according to Scheme 1 is then in excellent agreement with the experimental observations of 1.4–1.6 kcal/mol (Table 2).

A comparison of the averaged structures from the simulations with the crystal structure yields several interesting observations. First, the average root-mean-squared (rms) deviations for non-hydrogen atoms between the structures sampled for the complex of **1** and the crystal structure¹³ were computed. The average rms for the atoms in the side chains that were varied is 0.7 Å, and the average rms for the ligand **1** is 1.1 Å. The corresponding maximum rms values for individual structures did not exceed 0.8 and 1.4 Å, and the values at the end of the MC run were 0.7 and 0.9 Å. Thus, the MC sampled structures did not drift far from the crystal structure, though some differences emerged. In the α -ketoamide region of the ligand, the crystallographic interaction of O4 with an ϵ -hydrogen of Phe⁹⁹ is not maintained, but there is a frequent interaction of the ζ -hydrogen with the amide carbonyl oxygen (O3). The hydrogen bonds to Ile⁵⁶ and Tyr⁸² are unaffected by the perturbation (Figure 2). Within compound **1**, the 1-phenyl and isopentyl groups remain in contact. However, the 1-phenyl group moves away from Phe⁴⁶; the shortest contact between aromatic carbons increases from 4.5 Å in the crystal structure to 5.6 Å in the simulation. In both the crystal structure and from the

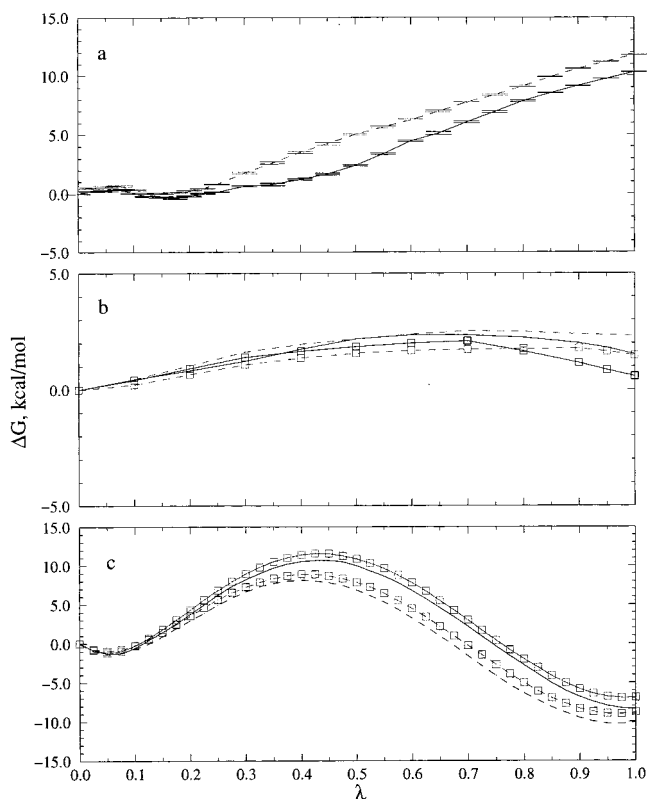


Figure 6. (a) Free energy profile for the transformation of **1**→**2**, with error bars for each window shown. (b) Profiles for **2**→**3** and **5**→**6** (squares). (c) Profiles for **2**→**5** and **1**→**4** (squares). Solid lines represent the unbound simulations, and the dashed lines result from simulations of FKBP12–ligand complexes.

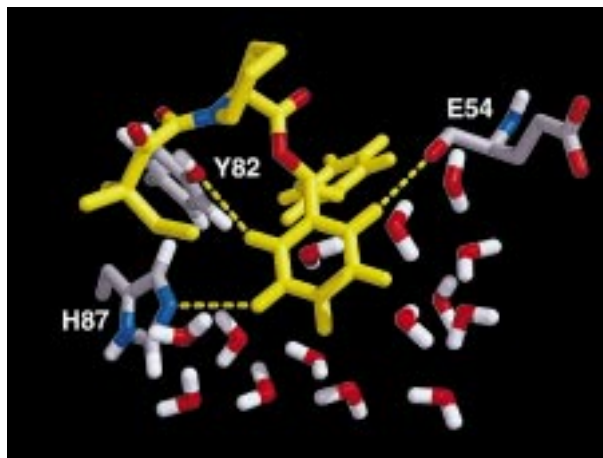
MC simulations, the 1-phenyl and isopentyl groups pack well into the hydrophobic pocket that is outlined by Phe⁴⁶, Phe³⁶, Ile⁹⁰, Ile⁹¹, Tyr⁸², and His⁸⁷ (Figure 2). Loss of hydrophobic contacts upon removal of the 1-phenyl group is unfavorable for binding.

The simulations also suggest that some specific contacts with the 1-phenyl group may be relevant. As highlighted in Figure 7, the 1-phenyl substituent makes aryl CH \cdots O contacts with the backbone oxygen of Glu⁵⁴ and the Tyr⁸² hydroxyl oxygen, and it has an amino-aromatic interaction with the ϵ -nitrogen of His⁸⁷. While the interactions of the 1-phenyl group in **1** with Tyr⁸² and Glu⁵⁴ are found in most of the structures analyzed, the interaction with His⁸⁷ occurs in only 29% of the analyzed structures. Average distances and frequencies

Table 2. Experimental Binding Free Energies, Calculated Free Energy Changes, and a Comparison of Experimental and Calculated Relative Binding Free Energies^a

A→B	exptl ^b		calcd		exptl ^c		calcd
	ΔG_A	ΔG_B	ΔG_{aq}	ΔG_{FKBP}	$\Delta \Delta G_b$	$\Delta \Delta G_b$	$\Delta \Delta G_b$
1→2	-10.6, -10.9	-9.0, -9.5	10.25 ± 0.31	11.69 ± 0.31	1.6, 1.4		1.4
2→3	-9.0, -9.5	-9.4, -9.2	1.52 ± 0.09	2.32 ± 0.08	-0.4, 0.3		0.8
5→6	-10.1	-11.1	0.59 ± 0.08	1.48 ± 0.07			0.9
2→5	-9.0, -9.5	-10.1	-8.36 ± 0.09	-10.07 ± 0.10	-1.1		-1.7
1→4	-10.6, -10.9	-9.9	-6.86 ± 0.11	-8.76 ± 0.11	0.7		-1.9

^a All free energies in kcal/mol. ^b Absolute binding free energies are derived from rotamase inhibition data given in Table 1, using $\Delta G = RT \ln K_i$ and $T = 25^\circ\text{C}$ (298 K). ^c Relative binding free energies are only listed when experimental data from the same source may be compared.

**Figure 7.** Intermolecular aryl CH···N, O contacts with His⁸⁷, Tyr⁸², and Glu⁵⁴ made in 1-FKBP12 that are lost on transformation to 2-FKBP12. One representative configuration from the Monte Carlo simulation is illustrated.

of occurrence of these and other key interactions between the ligands and FKBP12 are summarized in Table 3. Such aryl interactions are commonly observed in protein crystal structures, and their orientational distributions have been analyzed.^{55,56} To provide a sense of the strength of the aryl CH···X interactions with the OPLS-AA force field, gas-phase optimizations for complexes of benzene with phenol, imidazole, *N*-methylacetamide, and water yielded the interaction energies shown in Figure 8. With the hydrogen bonds constrained to be linear, the intrinsic interaction energies are in the 1–2 kcal/mol range.

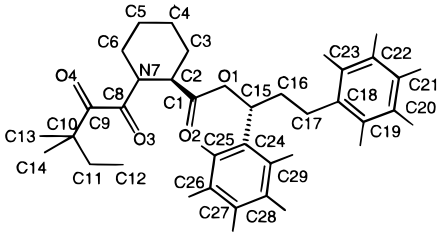
In both complexes, the 3-phenylpropyl moiety remains in the FK506-cyclohexyl region of FKBP12, and there is usually a water molecule well-positioned on the face of one or both phenyl rings in 1 (Figure 7). For reference, in the gas phase, the optimal π hydrogen bond between benzene and a water molecule has an interaction energy of ca. -3.5 kcal/mol.⁴² An aromatic hydrogen of the 3-phenylpropyl group often interacts with the carbonyl oxygen of Val⁵⁵ in 1-FKBP12; this contact is shorter and more frequent in 2-FKBP12 (Table 3). In addition, while the 1-phenyl ring no longer interacts with the Glu⁵⁴ backbone carbonyl oxygen when the transformation to 2 is complete, the 3-phenyl ring shifts to pick up this contact. Considering these observations, it is likely that the major contribution to the weaker binding for 2 than 1 is the overall reduction in hydrophobic interactions and, possibly, the specific loss of the aryl CH···O, N contacts between the 1-phenyl group and Tyr⁸² and His⁸⁷.

Effect of the 3-Phenyl to 3-(3-Pyridyl) Substitu-

tion, 2→3 and 5→6. Experimental data from Guilford Pharmaceuticals suggests that modification to a pyridyl substituent improves binding of 3-phenylpropyl compounds, although in one case this is contradicted by data obtained at SmithKline Beecham (Table 2). Considering the ca. 4 kcal/mol more favorable free energy of hydration of pyridine than of benzene⁵⁴ and assuming that the pyridyl compounds bind in a manner similar to 1 in the solvent-exposed region of the binding pocket, the phenyl to pyridyl conversion would be expected to decrease binding affinity. Simply put, a dipole is better solvated in a medium with a higher average dielectric constant.

First, the solvation of the ligands was addressed. The aqueous transformation of 2→3 resulted in a free energy difference of 1.52 ± 0.09 kcal/mol, somewhat larger than that for 5→6 (0.59 ± 0.08 kcal/mol). The gas-phase transformation of 5 to 6 yielded a free energy change of 3.15 ± 0.04 kcal/mol, which combines for a net relative free energy of hydration of -2.6 kcal/mol favoring 6. This is reasonable given the previous benzene to pyridine results,⁵⁴ and the larger, flexible ligand. Hydrogen bonds to water were similar for both sets of ligands; as expected, the pyridyl nitrogen provides an additional acceptor site in 3 and 6 (Table 4).

The free energy profiles for both pairs of unbound and bound perturbations are displayed in Figure 6b. They are again notably smooth. As seen from Table 2, the transformations in the protein are ca. 1 kcal/mol less favorable than those in solution, and the net result is a consistent preference for the phenylpropyl ligands. No direct protein contacts are made by the pyridyl nitrogen atom; its interaction with water is maintained (Table 4). For this hydrogen bond, the optimal interaction energy is -6.2 kcal/mol,⁵⁴ much stronger than an aryl CH···O- or N- interaction. However, the pyridyl nitrogen does participate in a hydrogen-bonding network with water molecules and carbonyl oxygens in the protein backbone. As reflected in Figure 9, a two-water bridge between the oxygen of Val⁵⁵ and the nitrogen is found consistently in 6-FKBP12. In 3-FKBP12 the interaction is often mediated by three water molecules, with a few structures in which one molecule also bridges to the Gln⁵³ carbonyl oxygen (Figure 9). The Val⁵⁵ oxygen has been noted previously as a consensus hydration site in FKBP12-ligand complexes.⁵⁷ Crystallographic waters from the 1-FKBP12 structure¹³ were not explicitly included in the calculations, so it is gratifying that this interaction is established during the MC simulations. Water surrounding the ligand in the binding pocket can also bridge longer distances; for example, in 6-FKBP12, four molecules link the hy-

Table 3. Key Intermolecular Hydrogen Bond Distances (Frequencies %) Less than 3.2 Å^a


FKBP12	ligand	1→2 ^b		2→3 ^c		5→6 ^c	
Tyr ²⁶ H ^ε	O4	3.0 (82)	2.8 (96)	2.7 (98)	2.9 (94)	2.8 (92)	2.8 (96)
Tyr ²⁶ H ^η	O4	2.8 (96)	2.9 (62)	3.0 (62)	2.9 (44)	3.1 (16)	3.0 (42)
Phe ³⁶ H ^ε	O3	3.0 (53)	3.0 (16)	3.0 (56)	3.0 (22)		
Phe ³⁶ H ^ε	O4	2.8 (93)	2.7 (96)	2.7 (96)	2.6 (98)	2.6 (100)	2.6 (98)
Gln ⁵³ O	H22					2.8 (96)	
Glu ⁵⁴ O	H23		2.8 (84)	2.8 (88)	2.8 (86)	2.8 (100)	2.9 (68)
Glu ⁵⁴ O	H25	2.8 (91)					
Val ⁵⁵ O	H21					3.1 (26)	
Val ⁵⁵ O	H22		2.7 (96)	2.8 (84)		3.0 (40)	
Val ⁵⁵ O	H23	2.9 (60)		3.0 (34)	3.1 (10)		2.9 (40)
Ile ⁵⁶ H	O2	2.0 (100)	2.0 (100)	2.0 (100)	2.1 (100)	2.0 (100)	2.0 (100)
Tyr ⁸² C ^ε	H19	3.0 (69)	3.0 (49)	3.1 (16)	3.0 (52)	3.0 (20)	3.0 (76)
Tyr ⁸² H ^ε	C19	3.1 (42)	3.0 (69)	3.1 (38)	3.1 (40)	3.0 (28)	3.0 (28)
Tyr ⁸² H ^ε	O3	2.9 (93)	3.0 (69)	3.0 (70)	3.0 (92)	3.0 (60)	3.1 (52)
Tyr ⁸² H ^η	O3	1.8 (100)	1.8 (100)	1.8 (100)	1.8 (100)	1.8 (100)	1.8 (100)
Tyr ⁸² H ^η	O1	3.1 (31)	3.1 (44)	3.0 (60)	3.0 (98)		3.0 (74)
Tyr ⁸² O ^η	H29	2.8 (93)					
His ⁸⁷ N ^ε	H28	2.9 (29)					
Phe ⁹⁹ H ^ζ	O3	2.9 (78)	2.7 (96)	2.6 (100)	2.8 (92)	2.9 (100)	2.7 (100)
Phe ⁹⁹ H ^ζ	O4					2.9 (22)	
Phe ⁹⁹ H ^ε	O4			2.9 (22)		2.9 (72)	3.0 (46)

^a Only interactions found in >10% of saved structures are reported. The frequency in parentheses records the percentage of the analyzed structures that had the feature. ^b 1→2 for 45 structures saved every 2 × 10⁵ configurations. ^c 2→3 and 5→6 for 50 structures saved every 2 × 10⁵ configurations.

droxyl oxygen of Tyr²⁶ to the backbone carbonyl of Glu⁵⁴ (not shown).

Finally, to ensure that the phenylpropyl 3-position selected for transformation did not influence possible protein–ligand contacts or the computed free energy difference, the final FEP window of 5→6 bound to FKBP12 was also started with the 3-pyridyl ring flipped by 180°. The free energy change calculated in this window was unaffected, and no new contacts with the protein were observed. In all, the simulations support the intuitive idea that binding for 3-(3-pyridyl)propyl compounds should be less favorable than that for 3-phenylpropyl ligands. This finding agrees qualitatively with the SmithKline observations for 3 and 2, but not with either pair of binding affinities (3 vs 2 or 6 vs 5) reported by Guilford Pharmaceuticals, as summarized in Table 2.

Effect of Ring Contraction on Binding, 2→5 and 1→4. With the relatively hydrophobic binding pocket of FKBP12, one might expect the larger pipercolyl compounds to bind with higher affinity than prolyl homologues. Though this is true for most published FKBP12 inhibitors,² the opposite pattern is reported for the 3-phenylpropyl and 3-(3-pyridyl)propyl compounds in Table 1.

With this in mind, the 2→5 transformation was pursued. The computed free energy change for the mutation unbound in water is -8.36 ± 0.09 kcal/mol (Figure 6c and Table 2). The corresponding perturbation was also performed in the gas phase and yielded a ΔG of -7.48 ± 0.03 kcal/mol. Combining the results gives a preference of 0.9 ± 0.1 kcal/mol for hydration of

the prolyl analogue, 5. The sign and small magnitude are consistent with experimental data for homologous hydrocarbons.⁵⁸ For the bound perturbation, the computed free energy change is -10.07 ± 0.10 kcal/mol (Figure 6c and Table 2). This combines with the aqueous result to predict stronger binding for 5 than 2 by 1.7 kcal/mol, which agrees well with the experimental difference of 1.1 kcal/mol.

The structure for 5–FKBP12 at the end of this simulation was very similar to that in the initial window of the 5→6 simulation. In both cases, the prolyl ϕ angle (C8–N7–C2–C1) of 5 was found to be -60° , while in all simulations of pipercolyl analogues the dihedral angle was ca. -90° . In addition, the prolyl rings in each 5–FKBP12 simulation reach slightly further into the binding pocket than do the larger rings, perhaps as a result of this dihedral change.

Having reproduced the unusual prolyl preference in the 2→5 FEP calculations, it was desired to test the calculations in a system where the experimental binding affinity of the prolyl analogue is reported to be less than that of the pipercolyl ligand. For the 1→4 conversion, the 1-phenyl substituent might prevent the 30° change in the prolyl ϕ angle and the deeper penetration of the binding pocket seen for 5, which could contribute to the reported binding preference of 0.7 kcal/mol for 1 (Table 2). The simulation was designed to perturb between the same ring conformations as in the 2→5 simulation, to serve as a “worst case scenario” for the 1,3-diphenylpropyl compounds. That is, 4 was predisposed to find the prolyl ϕ conformation of 5, unless prevented from doing so by the steric hindrance. From this perspective,

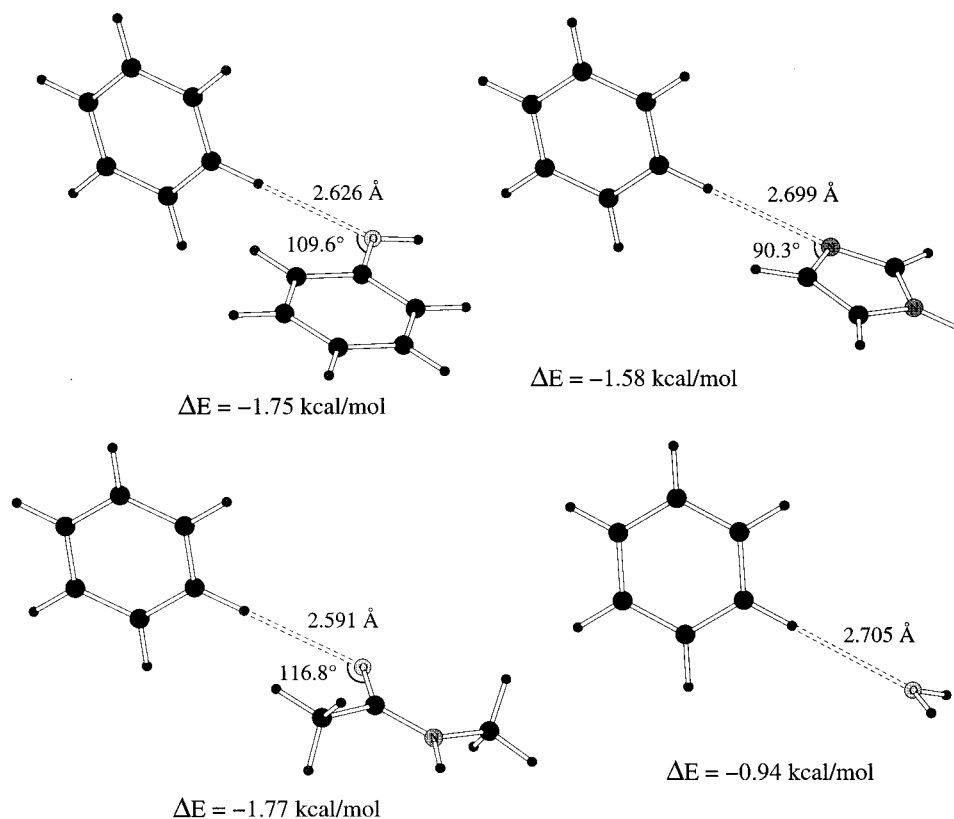


Figure 8. Results of constrained optimizations for linear benzene C-H...X interactions with OPLS-AA potential functions. Only the indicated variables have been optimized with the molecular planes orthogonal. The interaction energies are for formation of the complexes from the separated molecules. Results are shown for benzene with phenol, imidazole, *N*-methylacetamide, and water.

Table 4. Average Numbers of Interactions with Water Molecules in Unbound (Bound) Simulations^a

ligand atom	1-2	2-3	5-6
O1	0.0	0.0 (0.6)	0.0 (0.1)
O2	1.2	0.8	0.7
O3	0.8	1.0	1.0
O4	1.4	1.0	1.5
N _{pyr}	0.0	0.0	1.2 (1.0)

^a Only water molecules with an OH...X hydrogen bond length less than 2.5 Å and an interaction energy less than -2.25 kcal/mol with the solute were considered. For the bound ligands, only nonzero results are listed.

it is not surprising that the unbound and bound computed free energy changes for 1→4 parallel those of the previous ring contraction (Figure 6c), resulting in $\Delta\Delta G_b = -1.9$ kcal/mol. Thus, the calculations still favor the prolyl inhibitor, in contrast to the experimental binding preference for this ligand pair. The presence of the phenyl substituent, oriented away from the site of the mutation, did not materially affect the computed outcome.

The source of improvement for prolyl over the six-membered ring in both sets of simulations was then pursued. The largest contribution to the free energy difference in each window appears to come from changes in protein-ligand interactions, rather than solute-solvent or intramolecular interactions. The position of the prolyl ring in both 4-FKBP12 and 5-FKBP12 is such that atom C3 has moved to the position of C4 found in the pipercolyl analogues. This results in the loss of a close contact with atom C^{ε2} of Trp⁵⁹ (Figure 10). Inter-

estingly, based on the average C3-C^{ε2} distance in 1-FKBP12 of 3.5 Å, the close contact is unfavorable by 0.7 kcal/mol. Furthermore, atom C6, which carries a partial charge ($q_C = 0.285$) owing to its proximity to N7, is positioned 0.3 Å closer to the hydroxyl oxygen of Tyr²⁶ and its aromatic ring, a more favorable position from an electrostatic standpoint. The same is observed in the structures obtained from the 2→5 simulation.

While it may be that these interactions combine to improve affinity for prolyl rings in *this* binding mode, an alternate conformation not sampled in these simulations may also influence the binding affinities. One possibility is typified by FKBP12-bound crystal structures reported for the Vertex compound, V-10,367,²⁰ and a number of inhibitors developed at Agouron Pharmaceuticals¹⁷ that contain substituents which "fold over" the pipercolyl ring and interact primarily with Phe⁴⁶, in addition to or in place of substituents that fill the FK506-cyclohexyleth(en)yl groove of FKBP12. All that is required to reposition the 3-phenylpropyl arm of 1 in this manner, alongside the effector domain of FK506, is a rotation about the O1-C15 bond (Figure 11). A similar conformation was reported for the phenylalanine side chain of the Ace-Leu-Pro-Phe-Ame peptide in one theoretical study of the rotamase mechanism of FKBP12.³³ In that investigation, the solvent was treated as a continuum rather than as discrete molecules. Our simulations with explicit water molecules would not be expected to sample such a large conformational change for the ligand because the water structure would be too strongly disrupted for moves in this direction to be accepted with any regularity. This

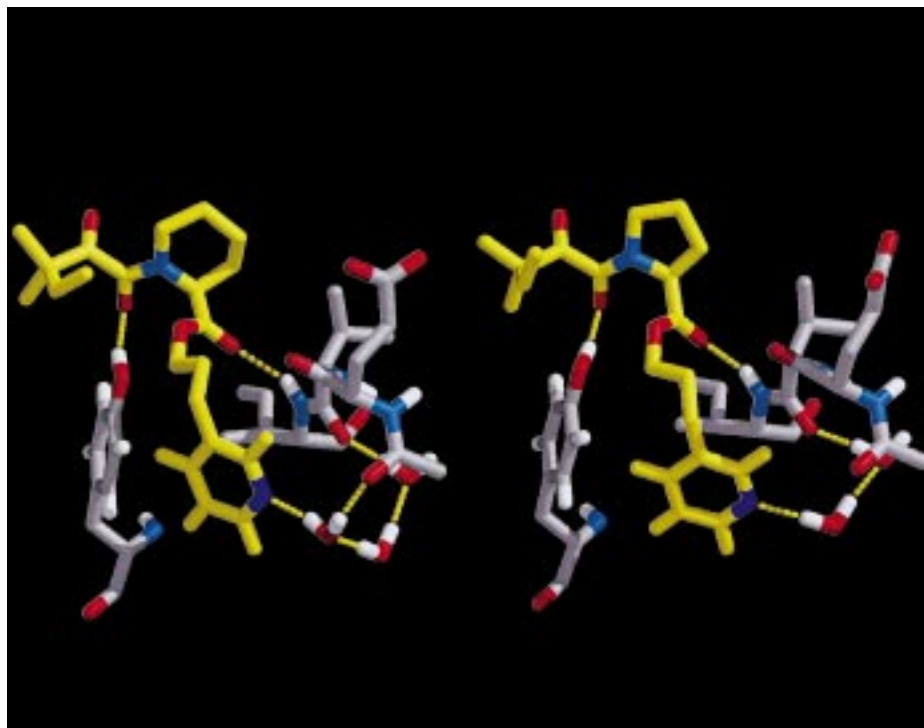


Figure 9. Illustration of bridging water molecules that modulate interactions between the pyridyl nitrogen and the protein backbone (Val⁵⁵ and Gln⁵³) in **3**-FKBP12 (left) and **6**-FKBP12 (right). Representative configurations from the Monte Carlo simulations are shown.

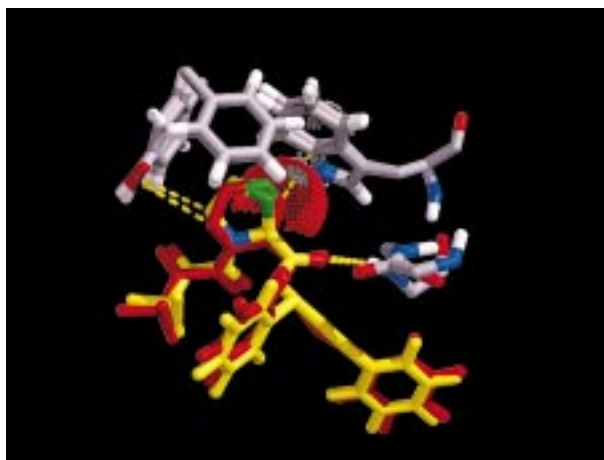


Figure 10. Pipecolyl versus prolyl ring binding in **1**-FKBP12 (red) and **4**-FKBP12 (yellow), representative of differences in analogous ligand pairs. The overlapping van der Waals surfaces of atoms C3 of **1** (red) and Trp⁵⁹C^{ε2} (gray) are shown. Atom C3 of **4** is positioned near C4 of **1** (both colored green) to relieve this unfavorable contact. Electrostatic interactions between C6 and Tyr²⁶O^γ are highlighted, and the position of Phe⁴⁶ and the intermolecular hydrogen bond to Ile⁵⁶ are also shown. Representative configurations from the Monte Carlo simulations are illustrated.

conformation would, however, permit the 3-phenyl or pyridyl rings to interact with Phe⁴⁶, which may confer some additional binding affinity. Inadequate sampling of alternate ring conformations for the unbound ligands may also be a particular concern for the present FEP calculations.

Conclusions

Overall, the present results further demonstrate the utility of Monte Carlo methods for sampling in free

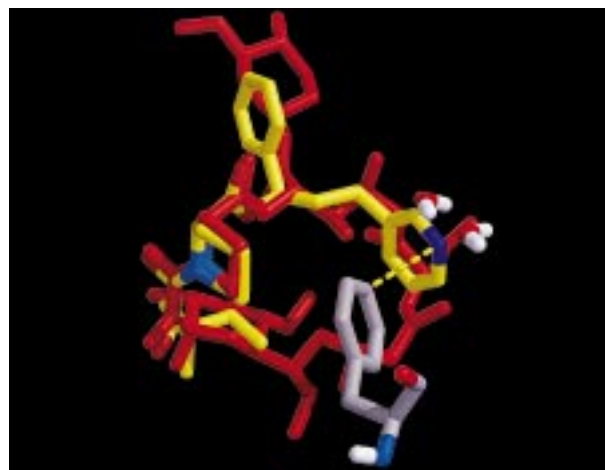


Figure 11. An alternative binding conformation possible for **1**. Interaction with Phe⁴⁶ can arise from rotation about the ligand O1–C15 bond from a dihedral of approximately 120.0° to –120.0°. The bound structure of FK506 is in red. (The orientation shown is rotated by 90° relative to Figure 3.) Two water molecules from the crystal structure of **1**-FKBP12 that would be displaced are displayed, as is one possible position of the nitrogen atom for the 3-pyridyl analogue.

energy perturbation calculations of protein–ligand systems. The computational removal of the phenyl group of **1** was straightforward, despite the large geometric perturbation. The corresponding reduction in binding affinity was attributed to the loss of hydrophobic contacts and, possibly, specific intermolecular aromatic CH \cdots N, O interactions. The results also suggest that **2**, for which no experimental protein-bound structure is available, binds similarly to **1** with FKBP12. Furthermore, a favorable contribution to binding reported for pyridyl substituents by Guilford Pharmaceuticals is not supported by the calculations using either pipecolyl

or prolyl ligands. However, the computed relative binding free energies for the pipicolyl compounds do agree with data from SmithKline Beecham and are consistent with the expected hydrophilicity of the pyridine nitrogen. Finally, improved binding of prolyl-containing compounds over the analogues with six-membered rings was predicted from the calculations. The results from perturbations of both **2**→**5** and **1**→**4** are consistent, favoring proline, although the binding of the latter compounds is reported experimentally to favor the larger ring. Removal of an unfavorable van der Waals contact with Trp⁵⁹ and improved contact with Tyr²⁶ were identified as contributors to the increased computed binding affinity. However, technical difficulties in path choice in this calculation were noted, and multiple solution or protein-bound conformations may unequally influence binding affinities of the ligand pairs. Modeling suggests that an alternative bound conformation may be possible for some of these ligands, positioning the 3-arylpropyl substituent in a region of space that coincides with the effector element of FK506 critical for calcineurin binding and immunosuppressant activity and in a position to interact with the Phe⁴⁶ residue of FKBP12. Such a position could be relevant for neurotrophic activity, if the activity results from binding an additional protein analogous to CN for immunosuppression.

Acknowledgment. Gratitude is expressed to Dr. Dennis A. Holt for helpful discussions, to Dr. Julian Tirado-Rives for important technical assistance, and to the National Institutes of Health for financial support. Many of the simulations were performed on a cluster of Pentium-based computers in our laboratory that were purchased with funds kindly provided by Pfizer, Inc.

Supporting Information Available: A listing of non-bonded and torsional parameters for the FKBP12 ligands (5 pages). See any current masthead page for ordering information and Internet access instructions.

References

- Fischer, G. Peptidyl-Prolyl *cis/trans* Isomerases and Their Effectors. *Angew. Chem., Int. Ed. Engl.* **1994**, *33*, 1415–1436.
- Hamilton, G.; Steiner, J. Neuroimmunophilin Ligands as Novel Therapeutics for the Treatment of Degenerative Disorders of the Nervous System. *Curr. Pharm. Des.* **1997**, *3*, 405–428.
- Rosen, M. K.; Schreiber, S. L. Natural Products as Probes of Cellular Function: Studies of Immunophilins. *Angew. Chem., Int. Ed. Engl.* **1992**, *31*, 384–400.
- Bierer, B. E.; Somers, P. K.; Wandless, T. J.; Burakoff, S. J.; Schreiber, S. L. Probing Immunosuppressant Action with a Nonnatural Immunophilin Ligand. *Science* **1990**, *250*, 556–559.
- Liu, J.; Farmer, J. D., Jr.; Lane, W. S.; Friedman, J.; Weissman, I.; Schreiber, S. L. Calcineurin is a Common Target of Cyclophilin-Cyclosporin A and FKBP–FK506 Complexes. *Cell* **1991**, *66*, 807–815.
- Griffith, J. P.; Kim, J. L.; Kim, E. E.; Sintchak, M. D.; Thomson, J. A.; Fitzgibbon, M. J.; Fleming, M. A.; Caron, P. R.; Hsiao, K.; Navia, M. A. X-ray Structure of Calcineurin Inhibited by the Immunophilin-Immunosuppressant FKBP12–FK506 Complex. *Cell* **1995**, *82*, 507–522.
- Kissinger, C. R.; Parge, H. E.; Knighton, D. R.; Lewis, C. T.; Pelletier, L. A.; Tempczyk, A.; Kalish, V. J.; Tucker, K. D.; Showalter, R. E.; Moomaw, E. W.; Gastinel, L. N.; Habuka, N.; Chen, X.; Maldonado, F.; Barker, J. E.; Bacquet, R.; Villafranca, J. E. Crystal Structures of Human Calcineurin and the Human FKBP12–FK506–Calcineurin Complex. *Nature* **1995**, *378*, 641–644.
- Cameron, A. M.; Nucifora, F. C.; Fung, E. T.; Livingston, D. J.; Aldape, R. A.; Ross, C. A.; Snyder, S. H. FKBP12 Binds the Inositol 1,4,5-Trisphosphate Receptor at Leucine-Proline (1400–1401) and Anchors Calcineurin to this FK506-Like Domain. *J. Biol. Chem.* **1997**, *272*, 27582–27588.
- Brown, E. J.; Albers, M. W.; Shin, T. B.; Ichikawa, K.; Kei, C. T.; Lane, W. S.; Schreiber, S. L. A Mammalian Protein Targeted by G1-Arresting Rapamycin-Receptor Complex. *Nature* **1994**, *369*, 756–758.
- Chiu, M. I.; Katz, H.; Berlin, V. RAPT1, a Mammalian Homolog of Yeast Tor, Interacts with the FKBP12/Rapamycin Complex. *Proc. Natl. Acad. Sci. U.S.A.* **1994**, *91*, 12574–12578.
- Sabatini, D. M.; Erdjument-Bromage, H.; Lui, M.; Tempst, P.; Snyder, S. H. RAFT1: A Mammalian Protein that Binds to FKBP12 in a Rapamycin-Dependent Fashion and is Homologous to Yeast TORs. *Cell* **1994**, *78*, 35–43.
- Choi, J.; Chen, J.; Schreiber, S. L.; Clardy, J. Structure of the FKBP12–Rapamycin Complex Interacting with the Binding Domain of Human FRAP. *Science* **1996**, *273*, 239–242.
- Holt, D. A.; Luengo, J. I.; Yamashita, D. S.; Oh, H.-J.; Konialian, A. L.; Yen, H.-K.; Rozamus, L. W.; Brandt, M.; Bossard, M. J.; Levy, M. A.; Eggleston, D. S.; Liang, J.; Schultz, L. W.; Stout, T. J.; Clardy, J. Design, Synthesis, and Kinetic Evaluation of High-Affinity FKBP Ligands and the X-ray Crystal Structures of Their Complexes with FKBP12. *J. Am. Chem. Soc.* **1993**, *115*, 9925–9938.
- Van Duyne, G.; Standaert, R.; Karplus, P.; Schreiber, S.; Clardy, J. Atomic Structure of FKBP–FK506, an Immunophilin-Immunosuppressant Complex. *Science* **1991**, *252*, 839–842.
- Van Duyne, G. D.; Standaert, R. F.; Karplus, P. A.; Schreiber, S. L.; Clardy, J. Atomic Structures of the Human Immunophilin FKBP-12 Complexes with FK506 and Rapamycin. *J. Mol. Biol.* **1993**, *229*, 105–124.
- Holt, D. A.; Konialian-Beck, A. L.; Oh, H.-J.; Yen, H.-K.; Rozamus, L. W.; Krog, A. J.; Erhard, K. F.; Ortiz, E.; Levy, M. A.; Brandt, M.; Bossard, M. J.; Luengo, J. I. Structure–Activity Studies of Synthetic FKBP Ligands as Peptidyl-Prolyl Isomerase Inhibitors. *Bioorg. Med. Chem. Lett.* **1994**, *4*, 315–320.
- Babine, R. E.; Bender, S. C. Molecular Recognition of Protein–Ligand Complexes: Applications to Drug Design. *Chem. Rev.* **1997**, *97*, 1359–1472.
- Gold, B. G.; Zeleny-Pooley, M.; Wang, M. S.; Chaturvedi, P.; Armistead, D. M. A Nonimmunosuppressant FKBP-12 Ligand Increases Nerve Regeneration. *Exp. Neurol.* **1997**, *147*, 269–278.
- Armistead, D. M. U.S. Patent 5 654 332, 1997.
- Armistead, D. M.; Badia, M. C.; Deininger, D. D.; Duffy, J. P.; Saunders, J. O.; Tung, R. D.; Thomson, J. A.; DeCenzo, M. T.; Futer, O.; Livingston, D. J.; Murcko, M. A.; Yamashita, M. M.; Navia, M. A. Design, Synthesis, and Structure of Non-macrocyclic Inhibitors of FKBP12, the Major Binding Protein of the Immunosuppressant FK506. *Acta Crystallogr.* **1995**, *D51*, 522–528.
- Hamilton, G. S.; Huang, W.; Connolly, M. A.; Ross, D. T.; Guo, H.; Valentine, H. L.; Suzdak, P. D.; Steiner, J. P. FKBP12-Binding Domain Analogues of FK506 are Potent, Nonimmunosuppressive Neurotrophic Agents In Vitro and Promote Recovery in a Mouse Model of Parkinson's Disease. *Bioorg. Med. Chem. Lett.* **1997**, *7*, 1785–1790.
- Steiner, J. P.; Connolly, M. A.; Valentine, H. L.; Hamilton, G. S.; Dawson, T. M.; Hester, L.; Snyder, S. H. Neurotrophic Actions of Nonimmunosuppressive Analogues of Immunosuppressive Drugs FK506, Rapamycin and Cyclosporin A. *Nat. Med.* **1997**, *3*, 421–428.
- Steiner, J. P.; Hamilton, G. S.; Ross, D. T.; Valentine, H. L.; Guo, H.; Connolly, M. A.; Liang, S.; Ramsey, C.; Li, J. H.; Huang, W.; Howorth, P.; Soni, R.; Fuller, M.; Sauer, H.; Nowotnik, A. C.; Suzdak, P. D. Neurotrophic Immunophilin Ligands Stimulate Structural and Functional Recovery in Neurodegenerative Animal Models. *Proc. Natl. Acad. Sci. U.S.A.* **1997**, *94*, 2019–2024.
- Crabtree, G. R.; Schreiber, S. L. Three-Part Inventions: Intracellular Signaling and Induced Proximity. *Trends Biochem. Sci.* **1996**, *21*, 418–422.
- Clackson, T. Controlling Mammalian Gene Expression with Small Molecules. *Curr. Opin. Chem. Biol.* **1997**, *1*, 210–218.
- Spencer, D. M.; Wandless, T. J.; Schreiber, S. L.; Crabtree, G. R. Controlling Signal Transduction with Synthetic Ligands. *Science* **1993**, *262*, 1019–1024.
- Spencer, D. M.; Belshaw, P. J.; Chen, L.; Ho, S. N.; Randazzo, F.; Crabtree, G. R.; Schreiber, S. L. Functional Analysis of Fas Signaling In Vivo Using Synthetic Inducers of Dimerization. *Curr. Biol.* **1996**, *6*, 839–847.
- Belshaw, P. J.; Spencer, D. M.; Crabtree, G. R.; Schreiber, S. L. Controlling Programmed Cell Death with a Cyclophilin-Cyclosporin-Based Chemical Inducer of Dimerization. *Chem. Biol.* **1996**, *3*, 731–738.
- Ho, S. N.; Biggar, S. R.; Spencer, D. M.; Schreiber, S. L.; Crabtree, G. R. Dimeric Ligands Define a Role for Transcriptional Activation Domains in Reinitiation. *Nature* **1996**, *382*, 822–826.

- (30) Liberles, S. D.; Diver, S. T.; Austin, D. J.; Schreiber, S. L. Inducible Gene Expression and Protein Translocation Using Nontoxic Ligands Identified by a Mammalian Three-Hybrid Screen. *Proc. Natl. Acad. Sci. U.S.A.* **1997**, *94*, 7825–7830.
- (31) Amara, J. F.; Clackson, T.; Rivera, V. M.; Guo, T.; Keenan, T.; Natesan, S.; Pollock, R.; Yang, W.; Courage, N. L.; Holt, D. A.; Gilman, M. A Versatile Synthetic Dimerizer for the Regulation of Protein-Protein Interactions. *Proc. Natl. Acad. Sci. U.S.A.* **1997**, *94*, 10618–10623.
- (32) Orozco, M.; Tirado-Rives, J.; Jorgensen, W. L. Mechanism for the Rotamase Activity of FK506 Binding Protein from Molecular Dynamics Simulations. *Biochemistry* **1993**, *32*, 12864–12874.
- (33) Fischer, S.; Michnick, S.; Karplus, M. A Mechanism for Rotamase Catalysis by the FK506 Binding Protein (FKBP). *Biochemistry* **1993**, *32*, 13830–13837.
- (34) Pearlman, D. A.; Connelly, P. R. Determination of the Differential Effects of Hydrogen Bonding and Water Release on the Binding of FK506 to Native and Tyr82→Phe82 FKBP-12 Proteins Using Free Energy Simulations. *J. Mol. Biol.* **1995**, *248*, 696–717.
- (35) Essex, J. W.; Severance, D. L.; Tirado-Rives, J.; Jorgensen, W. L. Monte Carlo Simulations for Proteins: Binding Affinities for Trypsin-Benzamidine Complexes via Free-Energy Perturbations. *J. Phys. Chem. B* **1997**, *101*, 9663–9669.
- (36) Pierce, A. C.; Jorgensen, W. L. Computational Binding Studies of Orthogonal Cyclosporin-Cyclophilin Pairs. *Angew. Chem., Int. Ed. Engl.* **1997**, *36*, 1466–1469.
- (37) Honig, B.; Nicholls, A. Classical Electrostatics in Chemistry and Biology. *Science* **1995**, *268*, 1144–1149.
- (38) Bernstein, F. C.; Koetzle, T. F.; Williams, G. J. B.; Meyer, E. F., Jr.; Brice, M. D.; Rodgers, J. R.; Kennard, O.; Shimanouchi, T.; Tasumi, M. The Protein Data Bank: a Computer-based Archival File for Macromolecular Structures. *J. Mol. Biol.* **1977**, *112*, 535–542.
- (39) Cheng, J.-W.; Lepre, C. A.; Chambers, S. P.; Fulghum, J. R.; Thomson, J. A.; Moore, J. M. ¹⁵N NMR Relaxation Studies of the FK506 Binding Protein: Backbone Dynamics of the Uncomplexed Receptor. *Biochemistry* **1993**, *32*, 9000–9010.
- (40) Lamb, M. L. Ph.D. Dissertation, Yale University, 1998.
- (41) Jorgensen, W. L.; Tirado-Rives, J. The OPLS Potential Functions for Proteins. Energy Minimizations for Crystals of Cyclic Peptides and Crambin. *J. Am. Chem. Soc.* **1988**, *110*, 1657–1666.
- (42) Jorgensen, W. L.; Severance, D. L. Aromatic-Aromatic Interactions: Free Energy Profiles for the Benzene Dimer in Water, Chloroform, and Liquid Benzene. *J. Am. Chem. Soc.* **1990**, *112*, 4768–4774.
- (43) Pranata, J.; Jorgensen, W. L. Computational Studies on FK506: Conformational Search and Molecular Dynamics Simulations in Water. *J. Am. Chem. Soc.* **1991**, *113*, 9483–9493.
- (44) Maxwell, D. S.; Tirado-Rives, J.; Jorgensen, W. L. A Comprehensive Study of the Rotational Energy Profiles of Organic Systems by *Ab Initio* MO Theory, Forming a Basis for Peptide Torsional Parameters. *J. Comput. Chem.* **1995**, *16*, 984–1010.
- (45) Allinger, N. L. Conformational Analysis. 130. MM2. A Hydrocarbon Force Field Utilizing V1 and V2 Torsional Terms. *J. Am. Chem. Soc.* **1977**, *99*, 8127–8132.
- (46) Mohamadi, F.; Richards, N. G. J.; Guida, W. C.; Liskamp, R.; Lipton, M.; Caufield, C.; Chang, G.; Hendrickson, T.; Still, W. C. Macromodel-An Integrated Software System for Modeling Organic and Bioorganic Molecules using Molecular Mechanics. *J. Comput. Chem.* **1990**, *11*, 440–467.
- (47) Yu, L.; Fesik, S. W. pH Titration of the Histidine Residues of Cyclophilin and FK506 Binding Protein in the Absence and Presence of Immunosuppressant Ligands. *Biochim. Biophys. Acta* **1994**, *1209*, 24–32.
- (48) Jorgensen, W. L. *MCPRO*, Version 1.5; Yale University: New Haven, CT, 1997.
- (49) Kofron, J. L.; Kuzmic, P.; Kishore, V.; Colón-Bonilla, E.; Rich, D. H. Determination of Kinetic Constants for Peptidyl Prolyl Cis-Trans Isomerases by an Improved Spectrophotometric Assay. *Biochemistry* **1991**, *30*, 6127–6134.
- (50) Weiner, S. J.; Kollman, P. A.; Case, D. A.; Singh, U. C.; Ghio, C.; Alagona, G.; Profeta, S., Jr.; Weiner, P. A New Force Field for Molecular Mechanical Simulation of Nucleic Acids and Proteins. *J. Am. Chem. Soc.* **1984**, *106*, 765–784.
- (51) Jorgensen, W. L. Computation of Free Energy Changes in Solution. In *The Encyclopedia of Computational Chemistry*; Schleyer, P. v. R., Allinger, N. L., Clark, T., Gasteiger, J., Kollman, P. A., Schaefer, H. F., Eds.; John Wiley & Sons Ltd.: Chichester, 1998, in press.
- (52) Kollman, P. Free Energy Calculations: Applications to Chemical and Biochemical Phenomena. *Chem. Rev.* **1993**, *93*, 2395–2417.
- (53) Zwanzig, R. W. High-Temperature Equation of State by a Perturbation Method. I. Nonpolar Gases. *J. Chem. Phys.* **1954**, *22*, 1420–1426.
- (54) Jorgensen, W. L.; McDonald, N. A. Development of an All-Atom Force Field for Heterocycles. Properties of Liquid Pyridine and Diazenes. *J. Mol. Struct. (THEOCHEM)* **1998**, *424*, 145–155.
- (55) Thomas, K. A.; Smith, G. M.; Thomas, T. B.; Feldman, R. J. Electronic Distributions within Protein Phenylalanine Aromatic Rings are Reflected by Three-Dimensional Oxygen Atom Environments. *Proc. Natl. Acad. Sci. U.S.A.* **1982**, *79*, 4843–4847.
- (56) Burley, S.; Petsko, G. Amino-Aromatic Interactions in Proteins. *FEBS Lett.* **1986**, *203*, 139–143.
- (57) Faerman, C. H.; Karplus, P. A. Consensus Preferred Hydration Sites in Six FKBP12-Drug Complexes. *Proteins: Struct., Funct., Genet.* **1995**, *23*, 1–11.
- (58) Ben-Naim, A.; Marcus, Y. Solvation Thermodynamics of Nonionic Solutes. *J. Chem. Phys.* **1984**, *81*, 2016–2027.
- (59) Hamilton, G.; Steiner, J. U.S. Patent 5 614 547, 1997.
- (60) Ferrin, T. E.; Huang, C. C.; Jarvis, L. E.; Langridge, R. The MIDAS Display System. *J. Mol. Graphics* **1988**, *6*, 13–27.

JM980062O